Scientific Motivations and Technical Design Considerations for Future High-Energy γ-ray Telescopes in Light of Lessons Learned from the Fermi Large Area Telescope.

Eric Charles[a]
on behalf of the *Fermi* Large Area Telescope Collaboration

[a]Kavli Institute for Particle Astrophysics and Cosmology, SLAC National Accelerator Laboratory, 2575 Sand Hill Road, M/S 29 Menlo Park, CA 94025, USA;

ABSTRACT

Five years into the *Fermi Gamma-ray Space Telescope* (*Fermi*) mission we have learned a great deal about the γ-ray sky, yet many open questions remain, and many new puzzles have arisen. In this contribution we will consider the science drivers for a variety of topics in high-energy gamma-ray astronomy, and how these drivers map into design considerations for future gamma-ray instruments in the energy range above 5 MeV. Specifically, we take the performance parameters and data set of the Large Area Telescope on the *Fermi* observatory (*Fermi*-LAT) as a baseline, and consider the scientific questions that could be probed by improving those parameters. We will also discuss the current state of detector technologies used in space-based γ-ray telescopes and discuss the magnitude of advances that would be required to make a future *Fermi*-like mission transformational enough to warrant the cost and effort. These summaries are intended to be useful for selecting technologies and making basic design decisions for future γ-ray telescopes.

1. INTRODUCTION

The Large Area Telescope on the *Fermi Gamma-ray Space Telescope* (*Fermi*-LAT, or just LAT) began science operations on 2008 August 4. Since then it has acquired by far the largest set of γ-ray data in the energy range from 20 MeV to over 300 GeV, which has enabled numerous advances in high-energy astrophysics.

The *Fermi* spacecraft and instruments do not have consumables, and, barring component failure or damage, could operate for over 25 years given the initial orbit. However, the wide field-of-view (FOV) of the LAT, combined with its sky-survey observation strategy, mean that continued operations will only increase the available statistics linearly with time for most parts of the sky. Several possible future high-energy γ-ray missions (i.e., sensitive to γ rays with energies above ~ 5 MeV) are in early phases of design and development and could benefit from considering the scientific questions that have been raised by results from the LAT. It is worth noting that these missions concepts feature a variety of detector technologies, include a Silicon tracker/ Tungsten converter similar to the LAT (GAMMA 400[1]), a Silicon tracker without conversion layers (Gamma-Light,[2] a Silicon PIN diode tracker (DAMPE[3]), a low-density gaseous time projection chamber (TPC, AdEPT[4]), a high-pressure gaseous TPC (HARPO[5]), and a liquid Argon TPC (LArGO[6]).

This paper is organized as follows: in Sec. 2 we will discuss the performance of the *Fermi*-LAT, taking it as a reference for future high-energy γ-ray missions; in Sec. 3 we will survey topics in high-energy γ-ray astronomy, and discuss which aspects of the instrument performance are most important for each topic; then in Sec. 4 we will discuss detector design considerations and available technologies for future high-energy γ-ray missions; finally, we will discuss and summarize our findings in Sec. 5.

2. SUMMARY OF FERMI-LAT PERFORMANCE

The LAT collaboration has published detailed descriptions of the LAT instrument,[7] the on-board calibrations[8] and performance.[9] Here we will provide a very brief overview of the key performance parameters. We will follow the notation conventions used in Ackermann et al. (2012).[9] For specificity we will refer to the most commonly used `P7REP_SOURCE` γ-ray selection and associated `P7REP_SOURCE_V15` instrument response functions (IRFs). It is important to note, however, that other event selections (e.g., `P7REP_TRANSIENT` or `P7REP_CLEAN`) are better suited to some particular analyses.

2.1 Background Rejection, Effective Area, Acceptance and Field of View

Background Rejection. Space-based γ-ray missions operating the in GeV energy range experience a background flux of cosmic rays 10^3 to 10^4 times the γ-ray flux. This cosmic-ray flux also produces some so-called "irreducible background", i.e., interactions in passive material near the instrument that produce a γ ray that scatters into the instrument that is indistinguishable from celestial γ rays.

With the LAT we were able to reduce the cosmic-ray background contamination to a small fraction of the celestial γ-ray flux while keeping over 50% of the γ rays that produced signals in both the tracker and calorimeter sub-systems across most of our energy range.

Effective Area. The effective area, $A_{\rm eff}(E,\hat{v})$, is the product of the geometrical cross section of the instrument and the efficiency to detect and select γ rays with a given energy (E) and incident direction ($\hat{v}$). For typical event selection criteria (i.e., the `P7REP_SOURCE` event class) the LAT $A_{\rm eff}$ peaks at about $0.8m^2$ for on-axis γ rays at 10 GeV. Fig. 1 summarizes the LAT $A_{\rm eff}$.

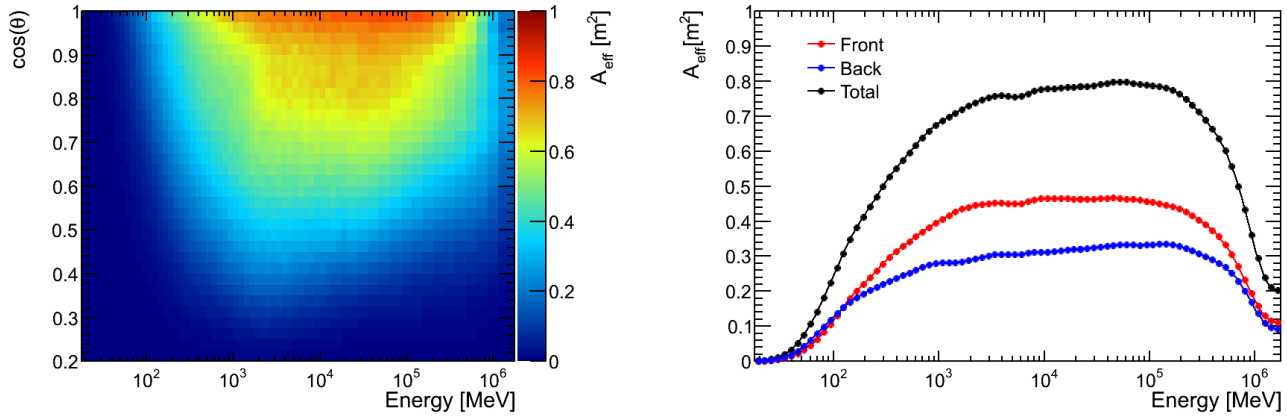

Figure 1. LAT $A_{\rm eff}$ in m^2 as a function of energy and off-axis angle (θ) (left), and as a function of energy for on-axis events (right). Front and back refer to events that convert in different sections of the tracker, which result in large difference in spatial and energy resolution.

Acceptance and Field of View (FOV). The acceptance (A) at a given energy is the integral of the $A_{\rm eff}$ over solid angle: $A = \int A_{\rm eff}(E,\hat{v})d\Omega$. For `P7REP_SOURCE_V15`, $A(E)$ peaks at around 2 m^{2}sr at 10 GeV.

We define the FOV as the ratio between the on-axis $A_{\rm eff}$ and A; e.g., the LAT FOV at 10 GeV is ~ 2.5 sr. Note that LAT is actually sensitive over a larger area; however the $A_{\rm eff}$ is much smaller towards the edges of the FOV. Fig. 2 summarizes the LAT acceptance and FOV.

Observing Strategy. The *Fermi* observing strategy has been to spend the large majority of time in "sky-survey" or "modified sky-survey" modes. In the former mode the LAT spends alternate orbits rocked 52° away from the zenith toward either the north or south orbital pole. With the wide FOV, this ensures complete sky coverage every two orbits ($\sim$ 3 hours). A few "modified sky-survey" modes have included pointing at specific targets with "sky-survey", or favoring either northern or southern rocking, to increase exposure to a particular source in that hemisphere.

2.2 Point-Spread Function, Point Source Localization Precision and Source Extension Sensitivity

Point-Spread Function. The point-spread function (PSF), $P(\hat{v}\,';E,\hat{v})$, is the probability density to reconstruct an incident direction $\hat{v}'$ for a γ ray with $(E,\hat{v})$.

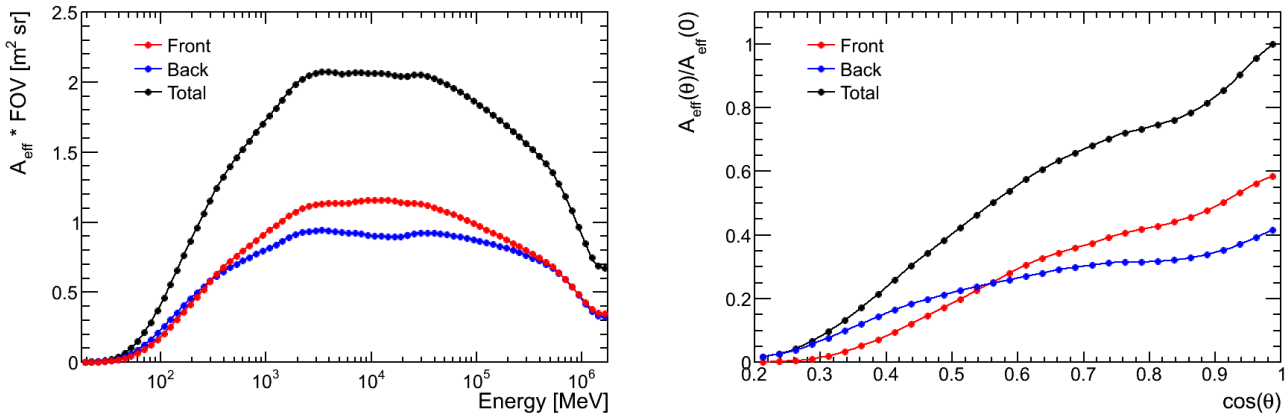

Figure 2. LAT Acceptance in m^2sr as a function of energy (left), and θ-dependence of the $A_{\rm eff}$ at 1 GeV (right).

For the LAT, the PSF varies markedly as a function of energy, being dominated by multiple Coulomb scattering (MCS) below a few GeV, and by the single hit resolution of the tracker at higher energies. Furthermore, the tails of the PSF are not Gaussian; the ratio of the 68% to 95% containment radii can be as large as $R_{95}/R_{68} \simeq 5$ for off-axis γ rays at high energies, where the event reconstruction is affected by so-called "backsplash" from the calorimeter.

Point Source Localization Precision. Appendix A of the second *Fermi*-LAT source catalog paper (2FGL[10]) describes a semi-analytic estimate of the localization precision, and finds the 95% CL localization radius to vary from 0.1° to 0.3° for sources near the detection threshold depending on the source spectrum. For stronger hard (see Fig. 3) sources localization radius scales with the detection significance (s) as $R_{95} = 0.34 \times s^{-0.68}$. Fig. 3 summarizes the LAT PSF and localization precision.

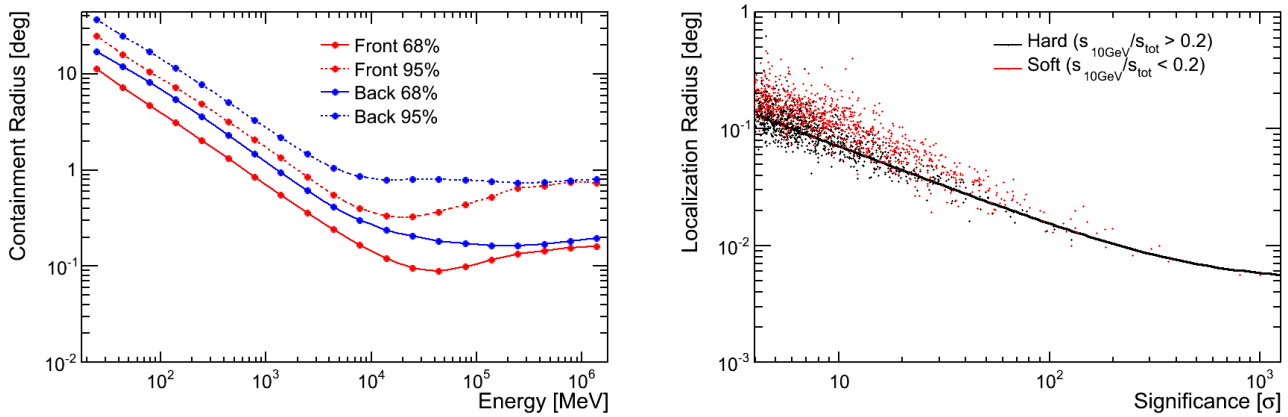

Figure 3. Containment radii of the acceptance-averaged PSF as a function of energy (left). LAT localization precision (given radius of the 95% error circle) as a function of source significance, values are taken from the 2FGL catalog (right). The solid line in the right plot shows a fit to the hard sources only, i.e., those sources for which the detection significance above 10 GeV is at least 20% of the total detection significance. The fit parameter values are given in the text.

Source Extension Sensitivity Detecting source extension depends on the flux and spectrum of the source in question and is easier for harder, brighter sources. Lande et al.[11] studied the LAT sensitivity to source extension in detail. To summarize the findings: establishing extension for sources smaller than 0.5° requires fluxes greater than the detection threshold, and only the very brightest LAT sources can be resolved as extended if the extension is smaller than $\sim 0.1°$.

2.3 Energy Bandpass, Energy Resolution and Spectral Resolution

Energy Bandpass. The LAT is sensitive to γ rays from 20 MeV to over 1 TeV. The lower limit is determined by the pair-conversion and Compton scattering cross sections, and by the requirement that the resulting particle leave signals in at least 3 tracker layers. Many analyses use a more stringent requirement that the particle deposit energy in the calorimeter, resulting in a large drop in $A_{\rm eff}$ below 100 MeV. The upper end of the range is determined by the finite depth of the calorimeter, above a few TeV the energy reconstruction breaks down.

In practical terms, the rapidly falling $A_{\rm eff}$, and worsening PSF and energy resolution at the lowest energies present significant challenges to extending spectral analyses of LAT data below 100 MeV.

Energy Dispersion and Energy Resolution. The energy dispersion, $D(E';E,\hat{v})$, is the probability density to measure an event energy E' for a γ ray with $(E,\hat{v})$. We define the energy resolution ΔE as the full 68% containment of the energy dispersion. Between from 1 GeV to 100 GeV, $\Delta E/E < 0.1$. Below 1 GeV, the energy resolution is degraded by energy losses in the tracker; above 100 GeV the energy resolution is degraded by the incomplete containment of the shower in the calorimeter (the 8.6 radiation length depth was limited by mass constraints).

Spectral Resolution. For sources with characteristic power-law spectra near the source detection threshold, the statistical uncertainty in the power-law index (Γ) is $\delta\Gamma \sim 0.2$. For stronger sources this uncertainty scales with the detection significance as $0.48 \times s^{-0.71}$. Fig. 4 summarizes the LAT energy resolution and the spectral index precision.

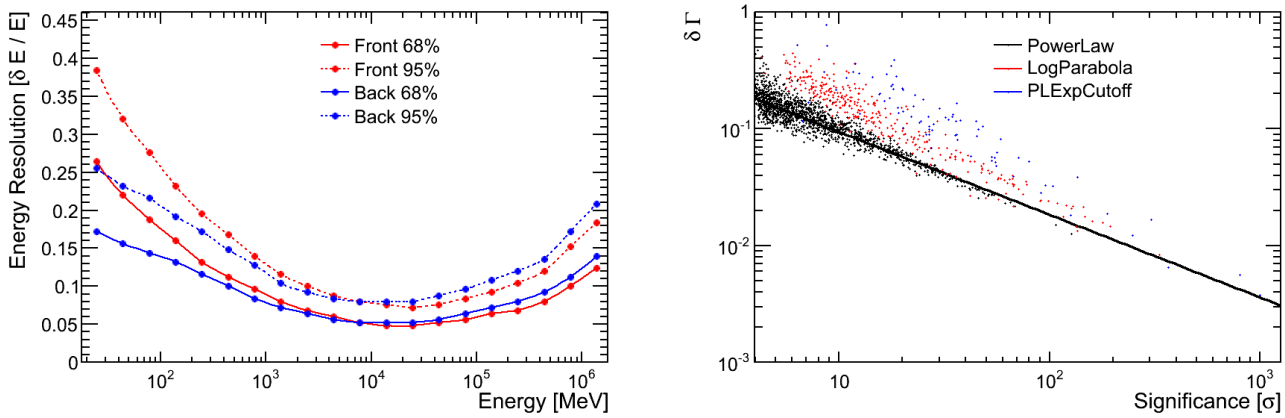

Figure 4. Acceptance-averaged energy resolution as a function of energy (left), and LAT spectral precision (i.e., the uncertainty on the power-law index) as a function of source significance; values are taken from 2FGL catalog (right). The solid line in the right plot shows a fit to the power-law sources only; the fit parameter values are given in the text. The additional free parameters in the other spectral forms result in larger statistical uncertainty in the spectral index.

2.4 Point-Source Sensitivity

Appendix A of the 2FGL catalog paper describes a semi-analytic calculation to estimate the LAT sensitivity to point sources. This calculation can be combined with maps of the diffuse γ-ray emission to estimate the flux threshold for detectability for a given spectral index across the sky, as shown in Fig. 5. It is also useful to extract the differential sensitivity, which is shown in Fig. 6.

Sensitivity to Variable Sources. By design the LAT can survey the entire sky every 2 orbits, or approximately every 3 hours. Only a few sources are detectable on such short time scales. Unsurprisingly, the time required to detect a source is highly correlated with the integral flux of that source, as shown in Fig. 7.

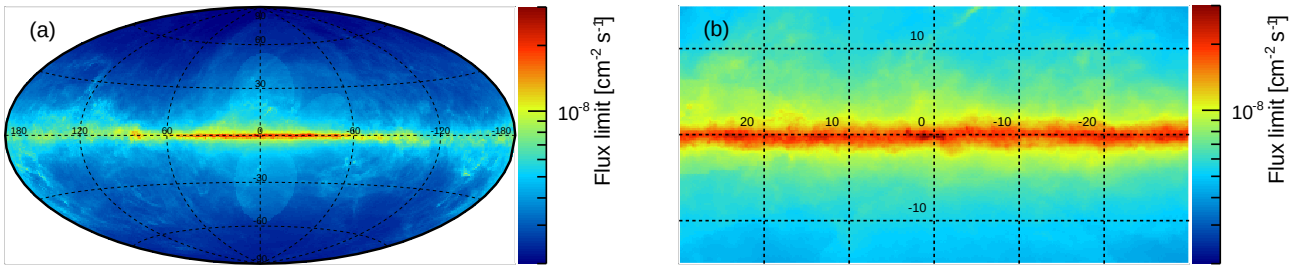

Figure 5. Flux above 100 MeV required for 5σ sensitivity for a point source with power-law spectrum with index $\Gamma = 2$. The calculation assumes a 4-year exposure. The entire sky (left) and a zoom on the Galactic center (right) are shown.

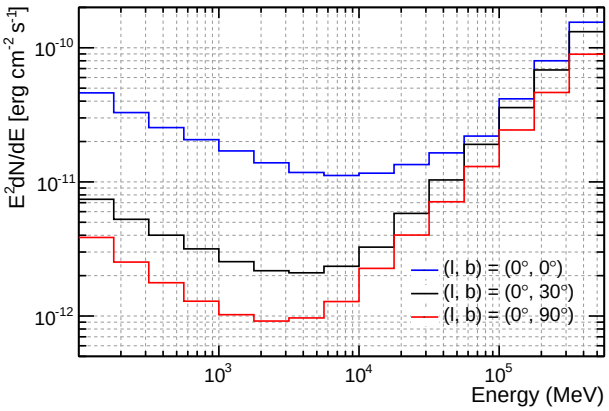

Figure 6. Differential sensitivity for a point source; the calculation assumes a 3-year exposure, 4 bins per energy decade. Requirements are 5σ sensitivity and at least 10 counts per bin. The sensitivity is shown at three locations in the sky: at the Galactic pole, at an intermediate latitude and on the Galactic plane.

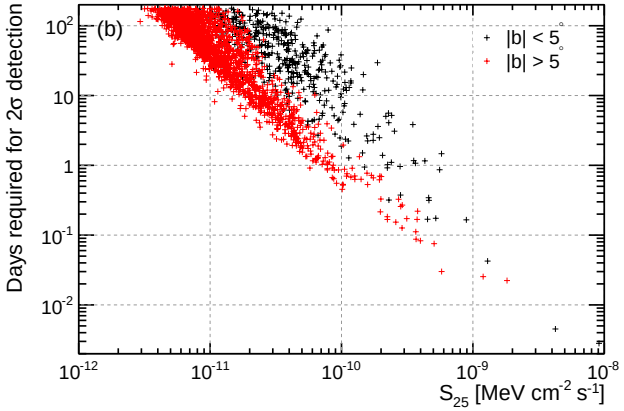

Figure 7. LAT sensitivity to variability of all 2FGL catalog sources, showing the estimated time required to reach a 2σ detection as a function of the integral energy flux between 100 MeV and 100 GeV (S_{25}) for both low- and high- Galactic latitude sources.

2.5 Other Performance Parameters

Several other important LAT performance parameters have to do with the timing of the event readouts. In particular the length of the window within which signals must arrive to be used in the triggering decision window ($\sim 0.7\mu$s), the minimum readout induced deadtime between triggers (26.5μs), the shaping time of the analog front-end electronics (varies from 3.5 to 10 μs between sub-systems) and the absolute timing accuracy ($< 1\mu$s).

Finally, it is worth mentioning the LAT's potential capability as a polarimeter, which was considered at several

points in the instrument design and was demonstrated in early simulations. However, practically speaking, the MCS from the tungsten converter foils makes it extremely difficult to extract the polarization signal, and only a small set of the brightest sources are potential targets for measuring polarization with the LAT.

3. SUMMARY OF SCIENTIFIC TOPICS AND GOALS IN γ-ray ASTRONOMY AND RELEVANT INSTRUMENT PERFORMANCE METRICS

A very broad range of astrophysical phenomena are accessible to the LAT, and will be available to future γ-ray missions. There are far too many results to cite here*, we will instead give a very abbreviated summary of the *Fermi* science topics, and how they are enabled by the instrument performance parameters.

3.1 Gamma-Ray Bursts (GRBs)

There are several outstanding scientific questions relating to GRBs. Indeed, the high-quality data from the *Fermi*-LAT and Gamma-Ray Burst Monitor (GBM) have shown several different spectral components and challenged simple models of GRBs. The γ-ray emission-mechanisms and the burst dynamics are subjects of active debate. Also, GRBs are valuable probes of intergalactic space over cosmological distances.

GRB Detection. The key performance parameters for detecting GRBs are the effective area and the FOV, particularly in the 10 MeV to 200 MeV energy range. Typically, the peak of the GRBs energy output is ~ 1 MeV, however they also exhibit delayed hard-spectrum emission extending over several hours. For the short timescales of GRBs, the background is small enough that the PSF is somewhat less critical. It is worth noting that increasing the FOV directly increases the odds that any one particularly bright GRB will be observed, and that a typical low Earth orbit will put the Earth's Limb at $\sim 110^\circ$ from the zenith, corresponding to an un-occulted sky fraction of $\sim 67\%$ or 8.4 sr. Relative to the LAT, important gains in GRB detection could be made by improving on the rapidly falling $A_{\rm eff}$ below ~ 300 MeV.

GRB Localization. The single most important aspect of GRB localization is that it be precise enough to facilitate multi-wavelength (MW) followup. The feasibility of MW followup depends on the FOV of the available instruments, as it is desirable that the localization region can be covered in a few pointings. In practical terms, a LAT localization of 1° or better will enable followup by the *Swift*-XRT[12] instrument. Successful detection by *Swift*-XRT in turn enables optical followup, which can identify the host galaxy and provide a redshift measurement. For the LAT, the localization is typically dominated by the few γ rays with the highest energies. This is because the PSF improves rapidly with energy up to the GeV range below which most GRB emission is detected. Relative to the LAT, marked gains could be made by improving the PSF in the low-energy regime where it is dominated by MCS, (see Sec. 4.1); however, almost all LAT localizations are precise enough to enable X-ray follow-ups. The scientific value of improved localization depends on the synergy with co-operating missions.

GRB Spectral and Temporal Modeling. The γ-ray fluence at the LAT varies dramatically between GRBs. For the purposes of spectral and temporal modeling of GRBs it is important to maximize the chance of observing the brightest GRBs; and to be able to continue observing them for as long as possible until they fade below detectability. Therefore, the field-of-view and the observing cadence are key parameters. The $A_{\rm eff}$, particularly at energies below 1 GeV is also key to maximizing the detected counts. Again, the soft spectra of GRBs in the LAT energy range suggest that marked improvements could be achieved by improving the acceptance below ~ 300 MeV. Finally, for the brightest GRBs, polarization measurements would be very useful in understanding the γ-ray emission mechanisms.

*A searchable, topic-indexed, bibliography of *Fermi*-related papers is maintained by NASA's *Fermi* Science Support Center, at `http://fermi.gsfc.nasa.gov/cgi-bin/bibliography_fermi`

Studies of the intergalactic medium, such as extra galactic background light (EBL) and Lorentz-Invariance violation (LIV). The γ rays from GRBs are useful as a probe of the intergalactic medium. Two particular types of studies have been made. 1) Deriving constraints on the γ-ray absorption caused by pair-production from γ rays interacting with the EBL, for which the key performance parameters are the effective area and the FOV, as the constraints are set by the highest energy observed γ rays. 2) Studies of LIV, i.e., setting constraints on the difference in arrival time and hence velocity differences between γ rays of different energies, for which the key parameters are also $A_{\rm eff}$ and the field of view, as the constraints are strengthened by observing a number of γ rays of different energies within a very short period of time. The timing resolution is also important, for resolving the shortest duration individual pulses within the GRB. Since both EBL and LIV constraints tend to be dominated by the highest energy detected γ rays, improving on LAT results would require larger acceptance and/or FOV above ~ 1 GeV, where the acceptance is limited primarily by the LAT geometry.

3.2 Galaxies

Since most galaxies are located away from the Galactic plane and have relatively low foreground diffuse γ-ray emission from the Milky Way, their study puts somewhat less importance on the PSF, and somewhat more importance on the source detection sensitivity and spectral resolution. However, there are some notable exceptions mentioned below where measuring source extension or morphology is important.

Active Galactic Nuclei (AGN). AGN have a wide range spectral properties, and many are highly variable, with variability down to timescales of down to minutes. Like GRBs, AGN have also been used as very sensitive probes of intergalactic space over cosmological distances.

1. AGN population studies. The key performance metrics are detection sensitivity (to reduce selection bias), localization precision (to help identify MW counterparts and facilitate redshift measurements), energy bandpass (to have a larger lever-arm for spectral fitting, including overlap with other instruments) and to a lesser extent spectral resolution, to better characterize spectral breaks. It is also worth mentioning that unresolved AGN comprise a large part of the so-called "isotropic" γ-ray background (IGRB, see Sec. 3.3) and increased detection sensitivity help resolve them from any truly isotropic backgrounds.

2. AGN variability. The key performance metrics are detection sensitivity, effective field-of-view, and observing cadence. These give increased sensitivity to flaring episodes and more continuous observations allow for higher quality light curves, of shorter time binning and smaller uncertainties flux in the time bins.

3. Studies of the intergalactic medium. Similarly to GRBs, AGN can be used to probe the intergalactic medium over cosmological distances. The key performance metrics here are the PSF (to measure or constrain the halo around AGN produced by the so called "pair-halo" effect, which gives information about the intergalactic magnetic field) and the metrics relevant for population studies (EBL studies have compared the spectra of a large set of well-understood blazars at known redshifts).

Improving the PSF at ~ 3 GeV by a factor of a few would increase sensitivity to the AGN pair-halo effect to source extensions smaller than 0.1°. Aside from that, γ-ray AGN science has entered the era of population studies of hundreds or more sources. We are likely to see sustained incremental improvements in our understand of AGN γ-ray emission as we use the population data to build and test models. Two areas stand out where such incremental improvements could lead to profound results. 1) Measurements of the EBL using γ rays have already started to constrain models of star formation at large redshift. 2) Current estimates suggest that unresolved AGN comprise a large portion of the IGRB. If correct this could tightly constrain the contributions from other sources, in particular dark matter (DM) contributions (see Sec. 3.6).

Finally, it is worth noting that measuring the γ-ray polarization in AGN, and observing changes in polarization during flaring episodes would provide extremely useful information for understanding the emission mechanisms of these sources.

Nearby Galaxies. In studying nearby Galaxies, the main performance metrics are the source detection sensitivity, the PSF (to study the morphology for those galaxies that can be resolved as extended sources) and the energy bandpass (to provide a large lever arm for spectral fitting). The primary potential for gain beyond the LAT lies in improving the PSF at lower energies, as that would both increase the detection sensitivity and the ability to study the morphology of these sources. This in turn would improve our understanding of the propagation of cosmic rays in galaxies.

3.3 Diffuse Emission and Cosmic Rays

Diffuse γ-ray emission comes primarily from three mechanisms: (1) π^0 decays from interactions between high-energy cosmic rays and interstellar dust and gas; (2) inverse-Compton up-scattering of starlight by high-energy cosmic rays; (3) Bremsstrahlung emission from electrons and positrons. Also, emission from populations of unresolved sources is effectively diffuse.

We can distinguish three main areas of research into diffuse γ-ray emission and cosmic rays.

1. Galactic diffuse emission. The PSF and the energy band-pass are key parameters for studying Galactic diffuse emission. The PSF is important to disentangle emission for different γ-ray emitting components, in particular in complicated regions, such as the inner Galaxy, along lines of sight down the spiral arms, and towards massive star-forming regions.

2. Isotropic diffuse emission. The key parameter for studying isotropic diffuse emission is rejection of cosmic-ray background, which is also isotropically distributed and difficult to disentangle from a population of isotropic γ rays. As second key parameter is the point-source detection sensitivity, as unresolved extragalactic sources will also contribute to the isotropic γ-ray component. It is also worth noting that the LAT measurement of the isotropic emission is statistics limited only at the very highest energies (> 1 TeV).

3. Cosmic rays. Although we are discussing γ-ray telescopes, it is worth noting that any γ-ray detector will also be sensitive to cosmic rays, and will require some amount of discriminating power to separate them from the γ rays. The main open questions affecting the scientific possibilities of measurements of cosmic rays are a) the energy resolution for hadronic interactions (as opposed to the electromagnetic interaction from γ rays, electrons and positrons), and b) the ability to discriminate between different cosmic-ray species.

By far the largest potential improvement over the LAT would come by improving the PSF, particularly at energies below 1 GeV. The MW maps used to provide templates for making the LAT diffuse γ-ray emission models generally have resolutions of 0.25° or better, which is much smaller that the LAT PSF below 1 GeV. Thus, currently, our ability to disentangle the individual components contributing to the diffuse γ-ray emission is limited by the LAT PSF, and in particular the large non-Gaussian tails of the PSF.

3.4 Galactic Sources

In general the PSF is a key performance metric when studying Galactic sources, because of the need to minimize potential source confusion, and to distinguish sources from the Galactic diffuse background. Pulsars, pulsar wind nebula (PWN) and supernova remnants (SNRs) are the main Galactic source classes, though several binary systems and a few Galactic novae have been observed to emit γ rays. There are several open questions about the γ-ray emission mechanism for each of these source classes.

Pulsars. Pulsars are excellent probes of General Relativity; millisecond pulsars in particular offer a laboratory to observe phenomena associated with extreme gravitational fields. Also, pulsar timing arrays are coming on line, and have good prospects for observing gravitational waves within the decade.

For studying pulsars, the synergy between γ-ray and radio observations is extremely important. Radio telescopes can detect pulsations with a single pointing, and dedicated monitoring campaigns can establish timing solutions. Furthermore, the radio and γ-ray fluxes are not particularly correlated, meaning that both bands play important roles in discovering new pulsars. Unlike in radio, γ-ray fluxes are small enough that many thousands of pulsation periods can elapse between the arrival of two γ rays. It is also important to note the difference between young pulsars, with periods in the 10 ms to 10 s range, and recycled millisecond pulsars (MSP) in binary systems, which have periods under 10 ms.

1. Pulsation Searches for Radio-Timed Pulsars. If a timing solution is available, key parameters for detecting pulsations are very similar to those for source detection. The timing solution can be used to phase fold γ rays, and PSF-weighting the γ rays by their observed angular separation from the pulsar can mitigate background contamination.

2. Blind Pulsation Searches. The key to detecting pulsations in "blind" searches (i.e., without a known timing solution) is to maximize the density in time of γ rays from the pulsar. Blind searches are very computationally expensive, and current state-of-the-art blind searches effectively use sliding time windows of the order of a week or less to form the initial candidate timing solutions. Furthermore, timing noise in young pulsars degrades the utility of combining data for periods longer than about a year. This in turn means that the $A_{\rm eff}$, FOV and observing cadence are key parameters for blind pulsar searches.[13] Because of the extra orbital parameters in binary systems, blind searches in γ rays for MSPs are extremely challenging, yielding only one MSP to date, and that search used optical data to constraint the binary orbital parameters.[14]

3. Targets for Radio Searches. Some more recent radio pulsar searches have adopted a strategy of simply aiming a radio beam at all unassociated LAT catalog sources. These searches have been quite successful, suggesting that the LAT's utility as a seed for radio searches is given by the same performance parameters as the source detection sensitivity.

4. Pulsar Timing and Modeling. While fruitful, efforts in modeling pulsars have not been able to explain the variety of observed pulsars. Increasing the timed pulsar population will help improve pulsar models. The key here is simply to time as many pulsars as possible, and to compare the radio and γ-ray pulse profiles. In essence, pulsar modeling will benefit from finding pulsations in timed radio pulsars, as well as finding new pulsars in blind searches and targeted radio observations. Although we cannot change the our viewing orientation of any particular pulsar, we can understand orientation effects, and the alignment of the pulsar magnetic field and spin axis, from measurements of a large population of pulsars.

Similarly to AGN, γ-ray pulsar science has entered the era of moderately large population studies, and we expect continued incremental improvements in our understanding. However, it is worth noting that most of the γ-ray pulsars observed to date are within 2 kpc of the Earth. Extending our effective horizon out to 8.5 kpc would be likely to result in a very large increase in the number of observed pulsar, as we start to probe the pulsar population near the Galactic center. This suggests a target of increasing the pulsation detection sensitivity by a factor of 15 to 20.

Additionally, observing a pulsar very close to the super-massive black hole at the Galactic center would allow for very precise tests of general relativity in the strong gravitational potential of the black hole.

Finally, observing polarization, and changes in polarization across the pulse period, would provide a very useful tool for locating the sites of γ-ray emission and testing pulsar models.

Supernova Remnants (SNR) and Pulsar Wind Nebulae (PWN) Important scientific questions in the study of SNR involve the interaction with the nearby medium, the γ-ray emission mechanism, and the role of SNRs as cosmic-ray accelerators. The morphology and the spectral precision (particularly near the 70 MeV π^0-decay threshold) are the two key aspects for resolving these questions. The large PSF and difficulty in performing spectral analyses below 100 MeV have made SNRs one of the most challenging sources classes to study with LAT data. Improving the PSF and energy resolution in that energy range would enable better separation and measurement of the hadronic component of the SNR shock by measuring the intensity of π^0 decay feature near 70 MeV. This in turn would improve our understanding of the energetics of SNR and help clarify their role as cosmic-ray accelerators.

Polarization aligned with the neutron star spin has been observed up to 1 MeV in the Crab PWN[15] and is expected at higher energies as well.

Binary Systems. Galactic binary systems have been observed in γ rays with periods ranging from days to years. All the systems have been highly variable in γ rays, and the emission mechanisms are still under debate. In fact the fluxes have been observed to vary by well over an order of magnitude across the orbital period. For studying binary systems, the key parameters are the detection sensitivity, field-of-view and observing cadence. The time-to-detect metric shown in Sec. 2.4 is particularly useful as the variability across the orbital period is key to modeling the γ-ray emission.

Galactic Novae. The LAT data have established Galactic novae as a new class of γ-ray emitters. These have been detectable for periods of days to weeks. As with many other source classes, the nature of the γ-ray emission mechanism is still under debate. To date only three Galactic novae have been observed in γ rays, so it is likely each new observation will provide additional surprises.

3.5 Emission from Objects in the Solar System

The Earth, Sun and Moon (and other objects in the Solar System) are targets for high-energy cosmic rays, and can be prolific γ-ray sources (in the case of the Earth and Sun). Furthermore, Solar flares and Terrestrial γ-ray flashes from lightning strikes can produce very bright transient sources of γ rays.

Cosmic-ray Interactions in the Solar System. By studying the γ-ray emission from the Earth, Moon and Sun (and potentially other objects in the Solar System), we can attempt to infer the spectra of the high-energy cosmic rays that produced these γ rays. The γ-ray spectra from the Sun and Moon are relatively soft, which places emphasis on the $A_{\rm eff}$ below ~ 1 GeV. On the other hand, the Earth's limb is an extremely bright source of γ rays, far outshining the rest of the sky. Having a large field of view, and a reasonably large $A_{\rm eff}$ near the edge of the field of view, enables taking Earth limb data without dedicated pointing. The Earth's limb is so bright that the spectrum can be measured extremely precisely. Below a few GeV features in γ-ray spectrum are related to the Geomagnetic cutoff of cosmic rays caused by the Earth's magnetic field, but at higher energies such features may be related to the primary cosmic-ray spectra.

It is also worth nothing that the Earth's limb is potentially a major source of contamination in any analysis. Improving the PSF increases the fiducial area usable for analyses.

Solar Flares. The mechanism for high-energy γ-ray emission from Solar flares is poorly understood. Solar flares have been observed in the LAT in two ways. First, directly, by detecting the sun as a γ-ray source for a period of minutes to hours. Second, indirectly, by observing increases in the rates in the scintillating tiles in the LAT anti-coincidence detector (ACD), as described in Appendix A of Ackermann et al. (2012). The ACD signature is likely due to piled-up signals from very large X-ray fluxes arriving within the shaping time of the front-end electronics. Unfortunately the ACD does not have sufficient timing and energy resolution to extract spectra from Solar flares, and the signals in the ACD are likely to cause the event classification algorithms to mis-identify γ rays that happen to arrive during the brightest X-ray Solar flares. This has precipitated work on event selections that make minimal use of the ACD and are more robust against high X-ray fluxes.

As an aside, the detection of Solar flares in the ACD raises the intriguing possibility of having a veto detector surrounding other sub-systems that functions as a transient γ-ray source detector and spectrograph in its own right.

Terrestrial Gamma-Ray Flashes (TGFs). TGFs are extremely intense bursts of < 30 MeV γ rays lasting < 1 ms associated with lightning strikes. They are observed in the LAT as a small number of sequential event readouts each with hundreds of individual signals in the LAT tracker. Although the direction and overall flux of the TGF can be estimated, it is generally not possible to distinguish individual γ rays within the TGF with the LAT. TGFs and the impulsive phase of Solar flares are the only two transient phenomena where the relative timing resolution (i.e., the front-end shaping time and the minimum time between event readouts) limit LAT measurements.

3.6 Searches for Signatures of Dark Matter (DM) and New Physics

There is a large body of research looking for indirect signatures of DM interactions in γ rays. Most of this research has focused on weakly interacting massive particles (WIMPs), i.e., non-standard model particle with masses in the 10 GeV to 1 TeV range. In many theories, the lightest non-standard model particle would be stable, but could self-annihilate into standard model particles, and the final state annihilation products could include γ rays. Robust theoretical arguments show that for WIMPs to explain the observed DM density, their thermally-averaged annihilation cross-section ($< \sigma v >$) must be near $3 \times 10^{-26}\mathrm{cm}^3\mathrm{s}^{-1}$. Analyses of LAT data have excluded these values of $< \sigma v >$ from DM particle masses less than ~ 30 GeV.

WIMP searches using LAT data have focused on a variety of targets.

1. Dwarf Spheroidal Galaxies (dSph). The dSphs represent the cleanest target for DM searches as they do not contain known γ-ray emitters and have reasonable estimates of their DM content. Thus, these searches are limited only by the detection sensitivity in the direction of the dSph. It is worth noting that, depending on the spatial distribution of the DM-related γ-ray emission, some dSph may be spatially extended LAT sources. Furthermore, in the case of a positive detection, spatially extended emission is a powerful discriminant between DM and other astrophysical sources. Resolving the spatial extension would increase the emphasis on the PSF.

2. Galaxy Clusters. Galaxy clusters differ from dSph in that they may include several astrophysical γ-ray emitters, as well as diffuse emission from cosmic-ray interactions in the cluster. The need to distinguish the emitters within the cluster makes the PSF somewhat more important than it is for the dSphs.

3. The Galactic Halo, Inner Galaxy and Galactic Center. Although the Galaxy represents the largest potential DM emitter, the large astrophysical foregrounds and uncertainties of modeling Galactic diffuse emission and unresolved sources makes the PSF key for disentangling DM from astrophysical contributions.

4. Spectral Lines. Searches for spectral lines from DM interactions producing monochromatic γ rays depend primarily on the energy resolution of the instrument. However, it is important to note that searches involving relatively large regions of the sky can easily become dominated by systematic uncertainties. In particular, at energies below ~ 10 GeV, very small ($\sim 1\%$) errors in modelling the LAT A_{eff} could result in highly significant ($> 5\sigma$) deviations from background models. Furthermore, misidentified cosmic-rays do not have the same energy dispersion as true γ rays and can fake or mask signals.

Improving on the LAT performance in WIMP searches depends on the spectrum of the WIMP-induced γ-ray emission, and hence on the mass of the WIMP, as well as on the search target. For many decay channels the γ-ray emission peaks at $\sim 10\%$ of the WIMP mass. For the relatively background-free dSph targets, the LAT analysis can be signal-limited at γ-ray energies as low as 10 GeV (WIMP masses of 100 GeV), while for the Galactic center, the analysis is background dominated up to 100 GeV (WIMP masses of 1 TeV) or more. Thus, as a rule of thumb, we can state that improving on LAT results for WIMP masses above 100 GeV using dSph would require improving on the acceptance, while analyses focusing on lower mass WIMPs, or the Galactic center, would benefit more by improving on the PSF. It is also worth noting that the Cerenkov Telescope Array (CTA[16]) will have a much larger A_{eff} for γ-ray energies above 50 GeV, as well as excellent spatial resolution. Taken together, these facts suggest that baring a detection by the LAT, DM searches in future high-energy γ-ray missions will be performed in updated theoretical frameworks motivated by non-detection in the LAT data.

3.7 Summary of Science Drivers

Tab. 1 summarizes the importance of the various instrument performance parameters for science topics in γ-ray astronomy.

Table 1. Summary of the importance of instrument performance parameters for science topics in high-energy γ-ray astronomy. Key performance parameter are marked as "1", other important parameters as "2", marginally relevant parameters as "3" and irrelevant parameters are unmarked. The performance parameters are background rejection ("Bkg"), point-source sensitivity ("Source"), on-axis $A_{\rm eff}$ ("$A_{\rm eff}$"), field-of-view (FOV), point-source localization ("PSF Loc."), extension detection/ associating a given γ ray with a particular source ("PSF Ext."), energy bandpass ("Band"), energy resolution ("Energy Res."), spectral resolution ("Energy spec."), relative timing and deadtime between readouts ("Timing Rel.") and absolute timing ("Timing Abs.").

			Acceptance		PSF		Energy			Timing	
Topic	Bkg.	Source	$A_{\rm eff}$	FOV	Loc.	Ext.	Band	Res.	Spec.	Rel.	Abs.
GRB Detection	2	1	1	1	3	-	2	-	-	-	-
GRB Localization	2	2	2	2	1	-	-	-	-	-	-
GRB Modeling	2	2	1	1	-	2	1	2	1	2	3
GRB EBL Studies	2	3	1	1	-	2	2	2	-	-	3
GRB LIV Studies	3	-	1	1	-	2	2	2	-	1	2
AGN Pop. Studies	3	1	1	2	1	-	1	3	2	-	-
AGN Variability	3	1	1	1	-	-	2	3	2	-	-
AGN EBL Studies	3	1	1	2	-	1	2	3	3	-	-
Nearby Galaxies	3	1	1	2	3	1	1	3	2	-	-
Galactic Diffuse	1	2	2	2	-	1	3	3	2	-	-
Extra-Galactic Diffuse	1	2	2	2	-	2	1	3	2	-	-
Radio Timed Pulsars	3	1	1	1	-	2	2	3	2	3	1
Blind Search Pulsars	2	2	1	1	1	2	2	3	2	3	1
Pulsar Radio Targets	3	1	1	2	1	-	3	3	3	-	-
Pulsar Modeling	3	2	1	2	-	2	2	2	1	3	1
SNR / PWN	2	2	1	2	3	1	1	2	1	-	-
X-ray Binaries	2	1	1	2	2	3	1	3	2	-	-
Galactic Novae	2	1	1	2	1	3	1	3	2	-	-
Earth	-	-	3	2	-	3	1	3	1	-	-
Sun / Moon	2	1	1	2	3	1	1	3	2	-	-
Solar Flares	2	1	1	1	1	3	1	3	2	2	-
TGFs	-	-	2	2	-	-	3	-	-	1	2
DM dSph	2	1	1	2	-	2	2	3	2	-	-
DM Galaxy Clusters	2	1	1	2	-	1	2	3	2	-	-
DM Inner Galaxy	3	2	2	2	1	1	1	3	1	-	-
DM Lines	1	-	2	2	-	3	1	1	1	-	-

Studying Tab. 1 confirms many things that we already knew. The keys to getting the best overall scientific return are improving the source detection sensitivity by maximizing the $A_{\rm eff}$ while minimizing the PSF. Having a large FOV and energy bandpass are also extremely important. The energy resolution is somewhat less critical, provided it is good enough to provide the spectral resolution needed to identify spectral breaks and cutoffs.

The real utility in Tab. 1 comes from considering where it is possible to make improvements with respect to the LAT. It would be quite easy to improve on the energy resolution, but aside from DM line searches, that would only marginally improve the scientific power on the instrument. At energies above ~ 1 GeV the LAT $A_{\rm eff}$ is primarily size-limited. This leaves us with three paths: 1) improving the PSF, 2) increasing the low-energy $A_{\rm eff}$, and 3) increasing the FOV.

Finally, it is worth emphasizing that γ-ray sky is much less well mapped in the 1-20 MeV range than at GeV energies. In fact, there is a roughly a factor of 10^3 difference in sensitivity between the LAT and COMPTEL,[17] the last imagining mission to operate in that energy range. Compared to the thousands of LAT sources, the COMPTEL catalog[18] lists 32 non-GRB sources.

4. CONSIDERATIONS AND LIMITATIONS RELEVANT TO THE DESIGN OF A HIGH-ENERGY γ-ray TELESCOPE

With the three goals stated at the end of the previous section, we turn to consider the physics that dictate instrument performance, and the current state-of-the art of potential detector sub-systems.

4.1 Summary of Relevant Particle Interactions with Matter

Above about 1 MeV the dominant processes of γ rays interactions with material are pair-conversion ($\gamma\gamma_{\rm virtual} \rightarrow e^+e^-$) and Compton scattering ($\gamma e^-_{\rm bound} \rightarrow \gamma e^-$). The dominant processes of electron and positron interactions with material are Bremsstrahlung and MCS. All of these processes are variants of the same Feynman diagram, and the cross-sections are of the same order of magnitude. An excellent summary of these processes is available in the Particle Data Group's "Review of Particle Properties" (PDG[19]). We will follow the notation used there. We also refer the reader to an excellent discussion of the challenge and benefits of measuring high-energy γ-ray polarization signals by Bernard (2013).[20]

Radiation Length. For a given material the radiation length (X_0, with units of gcm^{-2}) gives a characteristic scale for these interactions. The PDG gives a widely used approximation for X_0:

$$X_0 = \frac{716.4 \text{ g cm}^{-2} A}{Z(Z+1)\ln(287/\sqrt{Z})}, \tag{1}$$

where Z is the atomic number and A the atomic mass (in gmol^{-1}) of the material. Given the density (ρ) of the material the radiation length can then be expressed in cm. Silicon, for example, has a radiation length of $X_0\rho = 9.48$ cm.

Pair Conversion and Compton Scattering. The high-energy limit of the pair conversion cross section is related to X_0:

$$\sigma_{\rm pair} = \frac{7}{9}\frac{A}{N_A X_0}. \tag{2}$$

The majority of pair conversions occur in interactions with the electromagnetic field of the nucleus, the momentum transfer to the nucleus is not observed and sets a kinematic limit on the accuracy of the reconstruction of the γ-ray direction. Hunter et al. (2014[4]) have integrated the recoil momentum distribution to evaluate this kinematic limit. Fig. 1 of that paper shows the 68% containment radius obtainable from the kinematic limit alone, which scales roughly as:

$$\theta^{\rm limit}_{\rm pair,68} = 5^\circ (E/10 \text{ MeV})^{-1.2}. \tag{3}$$

However, about $1/Z$ of pair conversions occur with the electron field. In these cases, if the recoiling electron is observed in the instrument, the directional accuracy is only limited by the instrument resolution.

For comparison, in the high-energy limit, the Compton-scattering interaction length as a function of energy is:

$$X_{\rm Comp}(E) = \frac{13.0 \text{ g cm}^{-2}\text{MeV}^{-1} A}{\log(2E/m_e c^2) + 1/2} E \tag{4}$$

Comparison of Eq. (1) and Eq. (4) show that the energy at which pair-production starts to dominate over Compton scattering decrease markedly with the atomic number Z. Indeed, the energies at which the two processes balance are $\sim$ 3, 20, 50 and 80 MeV for Lead, Silicon, Carbon and Hydrogen.

The potential analyzing power of Compton-scatter events depends very much on the ability to measure the energy of the Compton-electron, and the position and energy of the γ ray after the Compton interaction, either when it is absorbed by a calorimeter "singles", or because of additional Compton interactions in the tracking volume ("multiples") before being absorbed in the calorimeter. Because of the much worse position resolution of calorimeters with respect to trackers, in practical terms, the PSF for singles is limited to $\sim 2^\circ$, whereas for multiples sub-degree PSFs are possible above a few MeV. On the other hand, undetected Compton-scattering will result in incorrectly reconstructed event energies.

In summary, below ~ 100 MeV Compton-scattering events can provide both a large boost in the $A_{\rm eff}$ and an equal or better PSF to pair-conversion events. Therefore, future high-energy γ-ray instruments should take them into account in their design. In particular, the performance for Compton-scattering events can be improved by minimizing the amount of passive material in the tracking and improving the energy resolution of the tracking detectors.

Energy Losses of Electrons and Positrons. Once an incoming γ ray has interacted, the energy loss of the resulting electrons and positrons due to bremsstrahlung is roughly:

$$\frac{dE_{\rm brem}}{dx} = \frac{E}{X_0}. \tag{5}$$

The critical energy (E_c), as defined by Rossi, is the energy at which the ionization loss per radiation length is equal to the electron energy, or alternatively, where the ionization loss is equal to the approximate for given in Eq. (5). Below E_c ionization losses will dominate very quickly and the electron or positron will lose the remainder of its energy linearly with distances traveled. The PDG gives these approximate relations for E_c:

$$\begin{aligned} E_c(Z) &= \frac{610 \text{ MeV}}{Z + 1.24} \quad \text{Solids,} \\ E_c(Z) &= \frac{710 \text{ MeV}}{Z + 0.92} \quad \text{Gases.} \end{aligned} \tag{6}$$

For the CsI crystals used in the LAT calorimeter, $E_c \simeq 11$ MeV.

Electromagnetic Shower Propagation. For relativistic electromagnetic showers the transverse extent of shower propagation is well characterized by the Moliére radius:

$$R_M = X_0 \frac{21.2\text{MeV}}{E_c}. \tag{7}$$

About 90% of the shower energy will be deposited within R_M and over 99% within $3.5R_M$. For typical calorimeter materials, R_M is a few cm and often sets the scale for the channel granularity for hodoscopic calorimeters.

For γ-ray induced showers, the maximum of the longitudinal energy deposition profile occurs at:

$$x_{\rm max} = X_0(\log(E/E_c) + 0.5). \tag{8}$$

In the case of incomplete shower containment, observing the shower maximum greatly improves the energy resolution achievable by fits to the longitudinal shower profile. For γ rays with 1 GeV (50 GeV) energy incident on CsI, $x_{\rm max} = 4.5X_0$ ($8.4X_0$). This sets the depth of the calorimeter.

Multiple Coulomb Scattering. The characteristic MCS angle, $\theta^{\rm rms}_{\rm space}$, for an electron or position with energy E traveling a distance x through a material can be approximated:

$$\theta^{\rm rms}_{\rm space} = \frac{\sqrt{2}\ 13.6 \text{ MeVrad}}{E} \sqrt{x/X_0}[1 + 0.038 \ln(x/X_0)]. \tag{9}$$

The scale of the prefactor is very important. In practical terms, it means for a 100 MeV particle, $\theta^{\rm rms}_{\rm space}$ will reach 0.62° after traversing $0.005X_0$. Using the radiation length of silicon given above, we see that this corresponds to only 470 μm, i.e., after traversing 1-2 planes of silicon. Put another way, achieving $\sim 0.62^\circ$ PSF resolution at 100 MeV would require somewhere between 100 and 200 readout points per X_0 of material in the tracking volume, depending on the geometry of converters and the sensors.

Angular Resolution Limiting Factor. In the absence of MCS, many position measurements would contribute to the directional precision, which would also improve linearly with the increased lever-arm. However, in practice, the measurements further along the direction of flight become increasingly affected by the MCS. We can estimate the detector thickness at which MCS dominates the directional measurement by finding when the directional precision from the first two measurements is equal to the multiple scattering angle for a single detector.

For two measurements of the position a particle, separated by a distance d, with uncertainties perpendicular to the direction of flight $\delta_\perp$, the directional uncertainty will be $\delta\theta_{\rm det} = \tan^{-1}(\sqrt{2}\delta_\perp/d) \simeq \sqrt{2}(\delta_\perp/d)$. For a detector geometry of stacked planes separated by a distance Δz, as in the LAT tracker, with resolution in the two planar dimensions of $\delta_{\rm plane}$, for a particle with incidence angle α with respect to the normal, this will give:

$$\theta_{\rm det} \simeq 2\frac{\delta_{\rm plane}\cos^2\alpha}{\Delta z}. \tag{10}$$

One factor of $\cos\alpha$ comes for the increased lever-arm, and the second comes from the projection of the measurement errors perpendicular to the flight direction.

One the other hand, for planar geometries the amount of material traversed increases as $\cos^{-1}\alpha$. If we ignore the small logarithmic correction factor in $\theta^{\rm rms}_{\rm space}$, this means that the detector thickness at which MCS dominates will be:

$$\frac{x}{X_0} \simeq (\frac{2\delta_\perp\theta^{\rm rms}_{\rm space}(\alpha=0)}{\Delta z})^2\cos^5\alpha. \tag{11}$$

The factor of $\cos^5\alpha$ is a challenge for large FOV designs with planar geometries, as it means that the optimal thickness of the planes varies by a factor of $2^{5/2} = 5.65$ (32) between normally incident particles and those arriving 45° (60°) off-axis.

4.2 Constraints for Space Missions

Space operations provide their own set of challenges for instrument design and operation. Here we will briefly discuss four of the most significant challenges: (1) power budget and heat dissipation, (2) data transmission rate, (3) use of consumables and reliability and (4) mass and size of the instrument.

Power Budget and Heat Dissipation. The power and head budget of a space-based observatory is severely constrained by the capacity of solar panels to provide energy, and the capacity of reasonably-sized radiators to dissipate heat. In practical terms this means that instruments must operate on a few kW of power. This limits the number of front-end electronics channels, as well as limiting the speed of the front-end electronics, as driving fast signals quickly requires significantly more power.

Data Transmission. A second constraint on space-based observatories is the available bandwidth for transmitting data to the ground. The LAT transmits roughly 16 GB per day, the vast majority of which is science event data. This corresponds to a data acquisition rate of roughly 185 kB s^{-1}, or less than 500 bytes per event at a readout rate of 400 Hz. It is worth noting that cost is the main limiting factor on bandwidth, i.e., bandwidth is expensive but available.

Consumables and Reliability. Any consumables will limit the mission lifetime, as will the failure of unreliable components. In practical terms, this somewhat disfavors the use of cryogenic systems that require a consumable coolant reservoir (as opposed to e.g., Stirling cycle engines that operate without consumables) and detector technologies that are susceptible to severe degradation from use or radiation damage.

Mass and Size. Obviously, a space-based observatory must be placed in orbit. This constrains both the mass and size of the observatory. Putting more mass into orbit requires larger, significantly more expensive, launch vehicles. Roughly speaking, the cost difference between a putting a 6000 kg payload (using, from example a Delta-II-H or proposed Ariane 6 vehicle) and a 20000-kg payload (using, for example a Delta IV-H or Ariane 5) into low Earth orbit is roughly $100 M.

4.3 Implications for Instrument Performance

It is useful to consider the instrument design as a series of trade-offs between performance parameters. Here we list several particular important design trade-offs that must be considered.

Background rejection versus FOV. It would be possible to obtain very large background rejection power by building a series of sub-systems to extract information useful for particle identification, such as time-of-flight detectors, Cerenkov imagers, magnetic spectrometers and so forth. However, requiring that a particle pass through each of the sub-systems would severely limit the FOV. It is also possible to improve the background rejection power by increasing the segmentation of the instrument, thus getting a more detailed picture of the events, and provide more information for the classification algorithms. However this increased segmentation comes at the cost of more channels and increased power consumption.

$A_{\rm eff}$ versus PSF. As discussed in Sec. 4.1, the cross-sections for pair-conversion, Coulomb- and Compton-scattering are all related. This implies that the single most-important design trade-off for high-energy γ-ray instruments: increasing the $A_{\rm eff}$ by adding material or increasing the density of the material will worsen the PSF. Similarly, increasing the distance between position measurements can improve the PSF outside of the MCS-dominated regime; however, given the size constrains of a space-mission, this will reduce both the $A_{\rm eff}$ and the FOV. It is worth mentioning as an aside that strategies such as active masks (e.g., a coded mask where the mask is instrumented with sensors which veto γ rays) could in principle achieve a much better PSF than the MCS limit, however, at the cost of a large reduction of the $A_{\rm eff}$ and FOV.

Sky-survey versus Pointed Observations The variety of trade-offs between the PSF and the $A_{\rm eff}$ and FOV suggest that a key design choice is between a sky-survey instrument and an instrument for pointed observations. The energy bandpass should factor heavily into this decision. The rapidly falling spectra of γ-ray sources limits the number of γ rays above a few GeV to the point that with an acceptance much smaller than the LAT, many science topics would be out of reach, even if the PSF is significantly better than that of the LAT. On the other hand, at lower energies, the complexity of the Galaxy combined with the much higher statistics favor an instrument with a better PSF, even at the cost of some $A_{\rm eff}$ and FOV. In short, a viable science case can be made for either a lower energy, small FOV, high-resolution pointed-mode, instrument spending most of the time scanning the Galactic Plane, or a slightly higher energy, survey mode instrument with the largest possible FOV.

PSF, Timing Resolution versus Power Budget. It is also worth noting that for many detector technologies, the spatial resolution can be improved by increasing the granularity of the sensor, and also by increasing the the readout time to decrease electronics noise. Conversely, increasing the timing resolution requires more power driving the front-end electronics. Clearly, a very large number of high-power consumption readout channels will quickly exceed the power budget.

Energy Resolution versus $A_{\rm eff}$ and FOV. Assuming the design includes a calorimeter (rather that an magnetic spectrometer, which would almost certainly limit the FOV), the energy resolution at high energies will be limited by the depth of the calorimeter, and at low energies by the mass in front of the calorimeter. Requiring that a γ ray deposit most of its energy in the calorimeter presents strong limitations on the effective usable fiducial volume, and will decrease some combination of the $A_{\rm eff}$ and the FOV.

Size versus Complexity of Event Readout, Triggering and Filtering. The LAT triggered readout rate was carefully tuned against the per-event deadtime to keep the overall deadtime at a reasonable 10%. Likewise, the data-reduction by the on-board filter was tuned to stay within the available bandwidth. The flux of cosmic-ray background through the instrument will increase with as the area of the instrument does, increasing the required complexity of the data acquisition and trigger systems.

Optimal Orbit. Because of the cosmic-ray screening from the geomagnetic cutoff, low Earth orbits have less cosmic-ray contamination. Similarly, equatorial orbits avoid the regions with the highest geomagnetic cutoff and also the south-Atlantic anomaly, where extreme radiation rates require shutting down sensitive instrumentation. On the other hand, significantly higher orbits reduce the FOV occulted by the earth, but also reduce the available payload mass for a given launch vehicle.

4.4 Sample of Detector Technologies

Most proposed future high-energy γ-ray telescopes designs rely on a few detector technologies: semiconductor-based solid state trackers, TPCs, hodoscopic crystal calorimeters and plastic scintillators and we will focus on those here. However, it is worth noting that three out of four of those detector technologies were used in the LAT design, and while technological advances have certainly been made since the LAT was built; for the LAT, significant improvement with respect to over previous missions came from switching from spark chambers used in EGRET and COS-B to Silicon strip detectors. Accordingly, we should not discount the potential for transformational application of new detector technologies to γ-ray astronomy. Again, we note that the PDG provides an excellent summary of available detector technologies.

Semiconductor-based solid state trackers. These include both strip and pixel detectors made from semiconductors such as silicon, germanium or diamond. All of these can achieve very precise positional accuracy, generally better than 30% of the channel pitch and as good as half that for detectors that use pulse height information to place hits between channels. Semiconductor detectors can also provide good measurements of the ionization energy deposited.

The limitation of these technologies are primarily geometrical. First, they they are generally built with thin flat planes, providing one measurement per plane (or two for double-sided detectors). The thickness of the planes is $> 200\mu m$, corresponding to $> 0.002X_0$ for particles at normal incidence, and increasing as the $\cos^{-1}$ of the incidence angle. Furthermore, the semiconductor wafers require support structures, increasing the X_0 per measurement. Second, they achieve high precision by having extreme segmentation, and the number of readout channels can grow very large and present challenges for the power and thermal budget and the available data transmission bandwidth (see Sec. 4.2). The 18 bi-layer LAT has 884k channels. Building an instrument with 200 layers of $0.005X_0$ each for a total of $1X_0$ of conversion target would increase that 100-fold. Furthermore, with the LAT's spatial resolution of $\sim 70\mu m$ the layers would need to be placed at least 2 cm apart to avoid degrading the PSF at 100 MeV. This would result in a 4 m tall instrument.

Time Projection Chambers. TPCs work by using a near uniform electric field to drift charge carries produced by ionization to the sides of the detector, where they are read out by sensor pads, which provide positional information in both direction transverse to the drift direction. Positional information in the longitudinal direction comes from measuring the drift time of the charge carriers.

Advances in solid-state sensor technology have made it possible to build very small individual channels on the amplification and sensor pads, allowing for excellent ($50\mu m$ or better) resolution in the transverse directions. However, the diffusion of the charge carriers limits the positional resolution in the longitudinal direction, particularly for large gas TPCs. With careful tuning of the drift gas longitudinal resolutions of $< 200\mu m$ for 1 m scale TPCs have been achieved.

TPCs can also quantify the ionization, which is useful for particle identification and quantifying the energy lost by charge particles in the TPC. The latter is particularly important for reconstructing Compton-scattering events.

One advantage of gas TPCs is that the density of the gas is low enough that several position measurement can contribute to the direction measurement, giving an excellent PSF. Furthermore, the density can be tuned to optimize the X_0 per-measurement. However, even the densest gases would require extreme pressures to provide enough target material for pair-conversion to reach LAT-like level; e.g., using Xe would require 50 bar of pressure at 300 K to reach $1X_0$/m. This suggests either segmented TPC cells with converter material between them, or placing converter material in the TPC.

Gas TPCs have other potential disadvantages. 1) The lower resolution in the longitudinal direction. 2) The difficulties in keeping the gas tuned for optimal performance. 3) The degradation of the gas and the readout sensor from chemical interaction between the two. 4) The difficulties in operating high-pressure gas systems in orbit. These last two suggest that the drift gas is potentially a mission-limiting consumable. On the other hand, it is worth noting that gas-based detection systems have been used successfully in several mission.

Solid-state (i.e., drift-detectors) or liquid TPCs offer less flexibility in tuning the X_0 per-measurement, but are also somewhat less difficult to operate in orbit. However, it is worth nothing that liquid Ar (as in LArGO) requires substantial cooling, potentially creating a mission-limiting consumable or increasing the heat load on the spacecraft radiators.

Hodoscopic Crystal Calorimeters Calorimeters for pair-conversion γ-ray mission have been homogeneous high-Z scintillating crystals. For ground-based calorimeters where the shower is largely contained, the energy resolution is usually parametrized as:

$$\frac{\sigma_E}{E} = \frac{a}{\sqrt{E}} \oplus b \oplus \frac{c}{E}, \tag{12}$$

where the first term represents stochastic and sample fluctuations, the second term comes from the calibration uncertainties, and the third term from the electronics noise in the channels contributing to the shower. Typical ground-based electromagnetic have 15 to 20 X_0, and can achieve resolutions as good as $2\%/\sqrt{E/1\mathrm{GeV}}$. Mass constraints for space missions coupled with the generally smooth spectra of astrophysical sources in the GeV range suggest using somewhat thinner calorimeters. The LAT, for example, is only $8.6X_0$ at normal incidence, and achieves energy resolution of better than 10% from 1 GeV to 100 GeV. Once the shower-maximum (Eq. (8)) is beyond the calorimeter depth, Eq. (12) breaks down with increasing energy.

Plastic Scintillators. Plastic scintillators are efficient, low-cost detectors. They have been used successfully as anti-coincidence charged particle vetoes in several γ-ray telescopes, and can provide particle background rejection factors better than to 10^4. Furthermore, the LAT has shown that segmenting the veto system can avoid "self-veto" from backsplash particles in high-energy γ-ray events.

As mentioned in Sec. 3.5, very high rates of X-rays are observed in the LAT ACD during bright solar flares. This raises the possibility of designing the readout system of any veto system so that it can double as a bright transient detector and spectrograph.

5. DISCUSSION

Reviewing Tab. 1 in Sec. 3.7 and considering the potential gains with respect to the LAT performance discussed in Sec. 3 we see three broad themes emerging, independent of the chosen technologies: 1) optimizing the PSF and 2) increasing the low-energy A_{eff} and 3) choosing the FOV, which impacts the instrument geometry.

Optimizing the PSF. The largest potential gains in many science areas come from improving the PSF, particularly at the lower energies in the MCS dominated regime (< 1 GeV). Furthermore, no space-based instrument can feasibly compete with CTA above ~ 50 GeV in terms of A_{eff} and detection sensitivity, which limits the need to extend the energy bandpass to the highest energies where almost all analyses would be signal-limited. This in turn suggests that for future instruments, the balance between improving the PSF or the A_{eff} should be pushed in favor of the PSF relative to the LAT. For a practical figure of comparison when considering instrument designs it would make sense to try and obtaining the best possible PSF while keeping the on-axis A_{eff} with a factor of two of the LAT over the energy bandpass of the instrument.

Interestingly, improving the PSF requires decreasing the MCS, which will also increase the sensitivity to polarization.

Increasing the Low-Energy $A_{\rm eff}$. The low-energy $A_{\rm eff}$ (i.e, below 100 MeV) of the LAT is limited primarily be three factors. 1) The falling cross section for pair-conversion. 2) The need to pass through 3-layer of high-density converter to leave enough hits to reconstruct a track. 3) The dearth of information about the event deposited in the detector, which makes background rejection much more difficult. Fortunately, these issues can be mitigated by including the measurement of Compton-scattering events in the instrument design and by reducing the MCS scattering in the tracking volume.

Choosing the FOV and the Instrument Geometry. The large FOV of the LAT and the all-sky survey mode it allowed has enabled many breakthroughs and is well-suited to the highly variable nature of many γ-ray emitting sources. It is worth recalling that the FOV of the LAT is 2.5 sr as compared to the un-occulted sky in low Earth orbit of 8.4 sr or 12.6 sr for the whole sky. Thus, the maximum potential gain in the FOV is somewhere between a factor of 3.5 to 5, depending on the orbit. Although not huge, this could be combined with a factor of 2 to 3 increase in the average effective area to obtain a factor of 10 increase in the acceptance without hugely increasing the size of the instrument, an important limitation in space missions.

On the other hand, the best ways to improve the PSF are to decreases the density of the material in the tracker and to space the tracking element further apart. Given the space limitations, both of these could result in a FOV that is somewhat smaller than the LAT's. These considerations present two alternate instrument geometries as opposite extremes to consider.

The first, designed to have an excellent PSF and a limited FOV, would be tall and relatively narrow, and maximize the lever-arm in the direction of travel of the incoming γ rays. Such an instrument would be suited to an observing strategy of scanning the Galactic plane with occasional pointings and limited surveys of high-Galactic latitude sources and regions.

The second, designed to maximize the FOV while retaining a very good PSF, would be as compact as possible for a given surface area, i.e., cubic or spherical. In this geometry, one of the challenges it so avoid building an intrinsic directionality into the instrument, e.g., a design with a tracker above a calorimeter is only sensitive to γ rays going "down", can not exceed a FOV 6.3 sr, and is unlikely to do better than about FOV 3 sr unless the tracker is extremely squat. So, in this case it is worth considering novel geometries, such a calorimeter sandwiched between two trackers.

An interesting alternative is the possibility of a "monolithic" instrument, i.e., one with a single sub-system that measures both the direction and energy of the incoming γ rays. In practice, this likely would be done in one of three ways, each of which would present substantial design challenges. 1) Adding a magnet to measure the momenta of the charged particles in the tracking volume. 2) Building a particle tracker that is several radiation lengths thick. 3) Increasing the readout granularity of a hodoscopic calorimeter to extent that it does not limit the PSF.

Summary We have presented a series of summaries of information that may be useful in the design of future high-energy γ-ray telescopes. Specifically, we have summarized the instrument performance factors critical for scientific goals, the physical mechanisms influencing the detector design, and the most popular detector technologies. We have also laid out the key trade-offs that must be considered.

Almost all of this information is available in greater detail elsewhere. However, we hope that this contribution will prove useful by consolidating the material in a single source.

ACKNOWLEDGMENTS

The *Fermi*-LAT Collaboration acknowledges generous ongoing support from a number of agencies and institutes that have supported both the development and the operation of the *Fermi*-LAT as well as scientific data analysis. These include the National Aeronautics and Space Administration and the Department of Energy in the United States, the Commissariat à l'Energie Atomique et aux Energies Alternatives and the Centre National de la Recherche Scientifique / Institut National de Physique Nucléaire et de Physique des Particules in France, the Agenzia Spaziale Italiana and the Istituto Nazionale di Fisica Nucleare in Italy, the Ministry of Education,

Culture, Sports, Science and Technology (MEXT), High Energy Accelerator Research Organization (KEK) and Japan Aerospace Exploration Agency (JAXA) in Japan, and the K. A. Wallenberg Foundation, the Swedish Research Council and the Swedish National Space Board in Sweden.

The author wishes to thank Stanley Hunter for pointing out an important mistake in Eq. (3) in previous versions of this contribution.

REFERENCES

[1] Galper, A. M. et al., "The Space-Based Gamma-Ray Telescope GAMMA-400 and Its Scientific Goals," *ArXiv e-prints* (June 2013).

[2] Morselli, A. et al., "Gamma-Light: High-Energy Astrophysics above 10 MeV," *Nuclear Physics B - Proceedings Supplements* **239-240**, 193–198 (2013).

[3] Fan, R. R. et al., "The silicon matrix for the prototype for the Dark Matter Particle Explorer," *ArXiv e-prints* (Mar. 2014).

[4] Hunter, S. D. et al., "A pair production telescope for medium-energy gamma-ray polarimetry," *Astroparticle Physics* **59**, 18–28 (2014).

[5] Bernard, D., "HARPO–A gaseous TPC for high angular resolution γ-ray astronomy and polarimetry from the MeV to the TeV," *Nuclear Instruments and Methods in Physics Research A* **718**, 395–399 (Aug. 2013).

[6] Caliandro, G. A. et al., "A new concept of y-ray telescope. LArGO: Liquid Argon Gamma-ray Observatory," *ArXiv e-prints* (Dec. 2013).

[7] Atwood, W. B. et al., "The Large Area Telescope on the Fermi Gamma-Ray Space Telescope Mission," ApJ **697**, 1071–1102 (June 2009).

[8] Abdo, A. A. et al., "The on-orbit calibration of the Fermi Large Area Telescope," *Astroparticle Physics* **32**, 193–219 (Oct. 2009).

[9] Ackermann, M. et al., "The Fermi Large Area Telescope on Orbit: Event Classification, Instrument Response Functions, and Calibration," ApJS **203**, 4 (Nov. 2012).

[10] Nolan, P. L. et al., "Fermi Large Area Telescope Second Source Catalog," *Astrophys.J.Suppl.* **199**, 31 (2012).

[11] Lande, J. et al., "Search for Spatially Extended Fermi Large Area Telescope Sources Using Two Years of Data," ApJ **756**, 5 (Sept. 2012).

[12] Burrows, D. N. et al., "The Swift X-Ray Telescope: Status and Performance," *ArXiv e-prints* (Mar. 2008).

[13] Dormody, M. et al., "Sensitivity of Blind Pulsar Searches with the Fermi Large Area Telescope," ApJ **742**, 126 (Dec. 2011).

[14] Pletsch, H. J. et al., "Binary Millisecond Pulsar Discovery via Gamma-Ray Pulsations," *Science* **338**, 1314– (Dec. 2012).

[15] Dean, A. J., "Polarized Gamma-Ray Emission from the Crab," *Science* **321**, 1183– (Aug. 2008).

[16] Actis, M. et al., "Design concepts for the Cherenkov Telescope Array CTA: an advanced facility for ground-based high-energy gamma-ray astronomy," *Experimental Astronomy* **32**, 193–316 (Dec. 2011).

[17] Schoenfelder, V. o., "Instrument description and performance of the Imaging Gamma-Ray Telescope COMPTEL aboard the Compton Gamma-Ray Observatory," ApJS **86**, 657–692 (June 1993).

[18] Schönfelder, V. et al., "The first COMPTEL source catalogue," A&AS **143**, 145–179 (Apr. 2000).

[19] Beringer, J. et al., "Review of Particle Physics (RPP)," *Phys.Rev.* **D86**, 010001 (2012).

[20] Bernard, D., "Polarimetry of cosmic gamma-ray sources above e^+e^- pair creation threshold," *Nuclear Instruments and Methods in Physics Research A* **729**, 765–780 (Nov. 2013).